Published in final edited form as:
J Bone Miner Res. 2015 January ; 30(1): 83–94. doi:10.1002/jbmr.2320.

Bone regeneration with osteogenically enhanced mesenchymal stem cells and their extracellular matrix proteins

Bret H. Clough[1,†], **Matthew R. McCarley**[2,3,†], **Ulf Krause**[2], **Suzanne Zeitouni**[1,3], **Jeremiah J. Froese**[1], **Eoin P. McNeill**[1], **Christopher D. Chaput**[2], **H. Wayne Sampson**[4], and **Carl A. Gregory**[1,*]

[1]Institute for Regenerative Medicine at Scott and White Hospital, Texas A&M Health Science Center, Module C, 5701 Airport Road, Temple, TX 76502

[2]Department of Orthopedic Surgery, Scott and White Hospital, Texas A&M Health Science Center, 2401 S. 31st Street, Temple, TX 76508

[3]University of Texas Medical Branch, Department of Orthopedic Surgery, 301 University Blvd. Galveston, TX 77555

[4]Department of Medical Physiology, Texas A&M Health Science Center, 702 Southwest H.K. Dodgen Loop, Temple, TX 76504

Abstract

Although bone has remarkable regenerative capacity, about 10% of long bone fractures and 25–40% of vertebral fusion procedures fail to heal. In such instances, a scaffold is employed to bridge the lesion and accommodate osteoprogenitors. Although synthetic bone scaffolds mimic some of the characteristics of bone matrix, their effectiveness can vary due to biological incompatibility. Herein, we demonstrate that a composite prepared with osteogenically enhanced mesenchymal stem cells (OEhMSCs) and their extracellular matrix (ECM) has an unprecedented capacity for the repair of critical-sized defects of murine femora. Furthermore, OEhMSCs do not cause lymphocyte activation and ECM/OEhMSC composites retain their *in vivo* efficacy after cryopreservation. We finally show that attachment to the ECM by OEhMSCs stimulates the production of osteogenic and angiogenic factors. These data demonstrate that composites of OEhMSCs and their ECM could be utilized in the place of autologous bone graft for complex orthopedic reconstructions.

*To whom correspondence should be addressed: cgregory@medicine.tamhsc.edu.
†Equally contributing authors.

Author contributions: CAG, CDC, and HWS designed research. BHC, CAG, CDC and MRM optimized the *in vivo* model. EPM, SZ, and UK performed tissue culture. BHC, CAG, EPM, SZ, and UK performed *in vitro* assays. BHC and CAG analyzed the μCT. BHC and JJF performed and interpreted histology. BHC and CAG co-wrote manuscript. All authors proof-read and approved the manuscript.

Data availability: Microarray data are available under GEO Series accession number [*pending*] (http://www.ncbi.nlm.nih.gov/geo/query/acc.cgi?acc=pending).

Conflict of interest: CAG is CSO of Blast Therapeutics Inc. CAG and Texas A&M University System filed two patents related to the technology reported in the manuscript. The other authors declare no competing financial interests.

Introduction

Although bone has a remarkable capacity for regeneration, approximately 10% of long bone fractures and as many as 25–40% of vertebral fusions fail to heal due to surgical technique (strength of fixation, soft tissue trauma) or host factors that impede healing like tobacco abuse (1–4). Osteoconductive scaffolds have a history as graft extenders to help bridge gaps between bones while reducing the need for autologus bone tissue. The most abundant of these materials is prepared from cadaveric bone tissue, but frozen materials present contamination issues and extensively processed allograft has reduced efficacy (5). A range of synthetic scaffolds have been developed, and although these products mimic some of the characteristics of bone, their effectiveness has proven highly variable (6, 7). More recently, strategies have utilized bone morphogenic protein (BMP) to promote/drive the differentiation of osteoprogenitors and induce bone formation (8). It can be effective, but in the case of vertebral fusion, BMP can cause harmful and even life threatening complications that may be related to pro-inflammatory effects (9, 10). Composites of bone marrow and bone-mimics are safer, but achieving reproducibility is challenging since success is contingent on the quality of the marrow (11). Autologous bone grafting, where bone is explanted from a distal site and implanted at the injury is very effective (12), but the available material is often insufficient and the additional surgery can cause significant morbidity.

The observation that autograft has a higher success rate than synthetics suggests that mimicry of anabolic bone is the key to generating an efficacious bone repair scaffold. This requires that osteogenic cells be present on an osteoconductive matrix. We have addressed this need by improving the osteogenic capacity of human mesenchymal stem cells (hMSC) by accelerating the canonical wingless (cWnt) pathway. This can be achieved by numerous methods (13) but we have exploited the crosstalk between peroxisome-proliferator-activated-receptor-γ (PPARγ) and cWnt signaling which regulates the adipogenic and osteogenic lineages respectively (14). When PPARγ is blocked by the inhibitor 2-chloro-5-nitrobenzanilide, GW9662 (15), inhibitory crosstalk on the cWnt pathway is released, thus enhancing osteogenesis (16). The resultant osteogenically-enhanced MSCs (OEhMSCs) generate an extracellular matrix (ECM) rich in collagens that are highly expressed in anabolic bone. The ECM has superior cell retention properties, and when administered with OEhMSCs, they exhibit an enhanced capacity for the repair of cranial lesions(17). Herein, we demonstrate that a scaffold prepared with OEhMSC-derived ECM and live OEhMSCs substantially improves the repair of critical-sized lesions in the femora of mice. We further demonstrate that attachment to the ECM by OEhMSCs stimulates the production of osteogenic and angiogenic factors including BMP2, through a mechanism involving collagens VI and XII. Finally, we show that OEhMSCs do not stimulate lymphocyte expansion when exposed to peripheral blood mononuclear lymphocytes (PBLs) and retain *in vivo* efficacy after cryopreservation. These data demonstrate that OEhMSCs and their ECM may represent a feasible allogeneic replacement for autograft in orthopedic procedures.

Materials and Methods (see Supplemental Methods for details)

Establishment of hMSC preparations

Under a Scott and White Hospital (Temple, TX) Institutional Review Board-approved protocol, bone marrow was recovered from the iliac crest of 2 hematologically healthy human donors. Using a previously published protocol, mononuclear bone marrow cells were subjected to a Ficoll discontinuous density gradient separation (18). Resultant buffy-coat cells were plated into 150 cm^2 tissue culture dishes (Corning Costar, Corning, NY) at an approximate density of 30,000 cells per cm^2 and cultured in complete culture media (CCM) consisting of alpha minimal essential medium, (alpha-MEM, GIBCO, Invitrogen, Carlsbad, CA) containing 20% (v/v) fetal bovine serum (FBS, Atlanta Biologicals, Norcross, GA), 2 mM L-glutamine, 100 units ml^{-1} penicillin and 100 μg ml^{-1} streptomycin (GIBCO, Invitrogen). Cells were incubated at 37°C in 5% (v/v) CO_2 and media were changed every 48 hr until a semi-confluent monolayer of fibroblastoid cells, free from hematopoietic cell contamination was generated. Cells were then recovered by trypsinization (GIBCO, Invitrogen) followed by cryopreservation in alpha-MEM containing 30% (v/v) FBS and 5% (v/v) dimethyl sulphoxide (Hybrimax, Sigma-Aldrich, St. Louis, MO). For each passage thereafter, cells were seeded at 100 cm^{-2} and expanded for 8–10 population doublings. Cells were used for experiments at passage 2. Phase contrast microscopy of cultures was performed using an inverted microscope (Nikon Eclipse, TE200) fitted with a Nikon DXM1200F digital camera.

Generation of OEhMSCs

OEhMSCs were generated as described previously (16, 17). Briefly, semi-confluent monolayers of hMSCs were incubated with OE-CCM media [CCM containing 5 mM β-glycerophosphate, 50 μg mL^{-1} ascorbic acid (Sigma Aldrich) and 0.1–10 μM GW9662 (EMD Millipore, Billerica, MA). Media were changed every 2 days and OEhMSCs were utilized for experiments at day 8.

Assembly of medullary pins

Twenty two and 19 gauge (G) surgical steel tubing was acquired from Small Parts Inc. (Miami Lakes, FL). Using digital callipers, the 22 G tubing was cut to exactly 9 mm length using a 1 mm thick, 22 mm diameter heavy duty cut-off wheel fitted to a Dremel rotary tool (Robert Bosch Tool Corporation, Mount Prospect, IL). The 19 G tubing was cut to 3 mm length. Burrs were removed using a latex polishing wheel and then polished with a cotton wheel. The 19 G tubing was positioned over the 22 G tubing at the exact center of the tube (Fig. S1A) and fixed with cyano-acrylate adhesive (Loctite, Henkel, OH). The 3 mm, 19 G collar acted as a spacer to maintain the size of the defect, to prevent slippage and penetration through the condyles, and to serve as a marker for the margins of the injury (Fig. S1B). Excess glue was removed with the polishing wheels. Where necessary, cylinders of surgical gelatin foam (Baxter, Deerfield, IL) were prepared by cutting 5 mm thick layers of Gelfoam (GF) with a cutting tool fashioned from 7 G surgical steel tubing. The resultant cylinders (5 mm length by 4 mm diameter) were pierced in the center and positioned over the 19 G spacer (Fig. S1C). In some cases, strips of GF was bioconditioned (see below) with OEhMSCs prior to cutting into cylinders. After reaming of the medullary canal with a blunt

21 G hypodermic needle, the pins fitted snugly into femora of 2 month old female nude mice with a good interference fit that resisted torsional motion. Micro-computed tomography confirmed that pins penetrated into the entire length of the medullary canal but did not cause significant damage to the metaphyseal trabecular bone (Fig. S1D).

Segmental defect and pin implantation

All vertebrate animal work was performed in accordance with an institutional animal use protocol approved by the Scott and White Hospital/ Texas A&M Health Science Center Institutional Animal Care and Use Committee (IACUC). Two month old (18–21 g) nude mice (Jackson Laboratories, Bar Harbor, ME) were housed under specific pathogen free conditions. A 3 mm pin-stabilized transverse femoral osteotomy was performed because a defect of this length was determined to be the minimum distance adequate to demonstrate experimental non-union in mice prior to our using the same pin design in the subsequent experiments. The skin over the lateral femur was incised for 5–10 mm along the longitudinal axis. Dissection through the muscle exposed the femur while taking care to preserve the posterior neurovascular bundle. A periosteal elevator was then used to further expose the central two thirds of the femur. Soft tissue was gently scraped from the bone with a scalpel, and dried with cotton gauze. The femora were handled using a pair of fine-nosed forceps previously fashioned in the Kern style to prevent excessive pressure on the bone (Fig. S1E). The central 3 mm section of femoral diaphysis was marked, and a dental drill fitted with a diamond coated rotary blade (0.1 mm by 8 mm) was employed to resect the marked portion of the femur. This was performed with copious saline irrigation to cool the bone. Medullary cavities were then reamed with a blunt 23G and then 21G hypodermic needle. The pin was then fitted into the proximal then distal medullary cavities to bring the femur back out to its original length and establish a stable 3 mm gap (Fig. S1D, F–H). Manual stress was then applied to achieve a good interference fit of the rod with the cortical bone of the femur. OEhMSCs were applied directly to the defect *in situ*. For this purpose, 2 million OEhMSCs were suspended in 25 μL reconstituted human plasma (Sigma-Aldrich) followed by addition of 25 μL of thromboplastin (Fisher Scientific, Pittsburgh, PA). The suspension was then quickly over-layed onto the defect and surrounding bone. The muscle and peripheral tissue was then be repositioned and closed with a continuous Biosyn 5-0 suture. The skin incision was then closed with 2–3 square knot Monosof 5-0 sutures and sealed with Vetbond adhesive. Mice rapidly recovered limb functionality.

Bioconditioning of Gelfoam

One million OEhMSCs were incubated in 10 mL of OECCM in 72.25 cm^2 low adherence tissue culture plates (Fisher) with 20 × 50 × 5 mm strips of Gelfoam (Baxter or Ethicon). Cells were allowed to adhere for 3 days with orbital shaking at 80 revolutions per minute. Media where changed every 2 days thereafter for 21 days. Gelfoam-MSC constructs were then processed as described previously (17). Briefly, the Gelfoam-MSC constructs were washed in excess PBS, and then frozen at −80°C for at least 24h. The constructs were then decellularized by lysis in buffer consisting of PBS containing 0.1% (v/v) Triton X100, 1 mM MgCl2, 10 μg/ml DNAse I, and 10 μg/ml RNAse A (Sigma) for 4 h at 37°C. The lysis was allowed to proceed for an additional 16 h in the presence of 0.125% (v/v) trypsin. The decellularized Gelfoam was then washed in dH2O and chloroform. Finally, ECM was rinsed

in 15 ml acetone and allowed to air dry. The processed ECM-rich material was hereafter referred to as *Bioconditioned Gelfoam* or BGF. In some experiments, the viability of OEhMSCs seeded onto either Gelfoam or BGF was evaluated using a commercial Live/Dead staining kit (Invitrogen) according to the manufacturer's instructions.

Micro-computed tomography (μCT) and analysis of murine femurs

After 2–3 weeks of healing, mice were humanely euthanized and the hind-limbs were dissected out taking care not to destroy the femoral head or damage the newly formed bone. Intact limbs were skinned and fixed in Carson's fixative for 7 days, washed in PBS, and wrapped in Parafilm. With the femur in the vertical orientation, the limbs were scanned at 30 kV/661 mA at 21 μm resolution using a Skyscan 1174 μCT unit (Bruker, Kontich, Belgium). Data were collected at 1° increments over the 360° with flat field, random movement and geometrical correction activated. After acquisition, the data were thresholded to a normalized scale developed using intact limbs from age-matched controls. Under these scanning conditions, the radiodensity of murine femur at the point of the defect corresponded to 500–5000 Hounsfield units. Axial images were then calculated using NRecon software (Skyscan). Regions of interest (ROI) corresponding to the volume of tissue between the proximal and distal edges of the collar were designated with the pin and a 0.5 mm margin subtracted. The volume and surface area of the bone tissue was calculated within the entire ROI using CTAn software (Skyscan). Polar moment of inertia (J) on 2D sections was calculated by taking the mean of 3 adjacent axial cross sections at the proximal end, distal end, and center of the injury using CTAn software. J was also calculated as the mean of the entire ROI. CTvol software (Bruker) was employed to generate 3D reconstructions from axial image data sets.

Histology

Following μCT scanning, hind limbs were placed in Carson's fixative (1.86% (w/v) sodium phosphate monobasic, 0.42% (w/v) sodium hydroxide, 10% (v/v) formaldehyde at 4°C until decalcification. For this purpose, limbs were washed with fresh PBS and decalcified in 0.5 M dibasic EDTA at pH 7.2 (Sigma), with changes every two days until radiolucency. The pin was then carefully removed. Processing and embedding of tissue involved manual dehydration through an ascending gradient of alcohols, clearing with Sub-X clearing agent (Surgipath medical industries, Inc.; Richmond, IL) and infiltration with paraffin wax (Tissue Prep 2, Fisher Scientific). Paraffin-embedded hindlimbs were cut in 10 μm thick sections and floated onto Histo-bond microscope slides (StatLab). Sections were baked onto slides at 60°C for one hour before clearing with citrus clearing agent (Richard-Allan Scientific) and rehydration with distilled water. Masson's trichrome staining was performed using a commercially acquired kit (American Mastertech Scientific Inc., Lodi, CA). Permount with toluene (Fisher Scientific) was used as a mounting medium. Micrographs were generated using an upright microscope (Nikon Eclipse 80i fitted with a Retiga 2000 camera) running digital imaging software (Elements, Nikon).

Calvarial defect model

The calvarial defect model was performed using 3 week-old female nude mice acquired from Jackson Laboratories according to a previously described, IACUC approved procedure (16, 17).

Statistics

Multiple pairwise comparisons within data-sets were analyzed using one-sided ANOVA followed by Tukey post-test. Single statistical comparisons were performed using the Student's T-test. Statistical analysis of bridging data was performed using the Fisher exact test. Fold-change PCR data were arcsine-transformed prior to statistical testing. *P* values below 0.05 were designated statistically significant in all cases. Statistical tests and data plotting were performed using GraphPad Prism version 5.00 for Windows (GraphPad Software, San Diego, CA).

Results

Characterization of OEhMSCs

hMSCs were cultured from human bone marrow as previously described [(18)]. Cells were positive for mesenchymal markers and negative for hematopoietic markers (Fig. S2A). The hMSCs also generated osteoblasts, adipocytes and chondrocytes (Fig. S2B–I), confirming that the cells met the minimal criteria for hMSCs (19).

OEhMSCs were generated from the hMSCs by incubation with GW9662 (16, 17). OEhMSCs exhibited a dose-dependent increase in OPG secretion (Fig. 1A) ALP activity (Fig. 1B), and mineralization capacity (Fig. 1C). They also retained a mesenchymal immunophenotype (Fig. 1D). To confirm lack of immune-stimulatory properties, OEhMSCs were co-cultured with peripheral blood lymphocytes (PBLs) labeled with carboxyfluorescein-succinimidylester (CFSE). While stimulated PBLs proliferated, resulting in dilution of the CFSE, unstimulated PBLs and PBLs in the presence of OEhMSCs failed to proliferate (Fig. 1E), suggesting that OEhMSCs are unlikely to elicit immune responses in human recipients and probably other species. Nevertheless, because the main goal of the study was to assess efficacy in bone repair, *in vivo* experiments were performed in immune-compromised nude mice.

OEhMSCs and healing murine femora

In our previous studies, OEhMSCs were superior to hMSCs for repair of calvarial defects (16, 17). We therefore speculated that OEhMSCs might be advantageous for repairing long bones. We generated a pin-stabilized critical-sized segmental defect in the femora of nude mice (Fig. S1) and administered 2×10^6 OEhMSCs to the defect with clotted human plasma. After 3 weeks, hind-limbs were subjected to micro-computed-tomography (μCT) and histology. In the case of untreated defects or those treated with hMSCs, we observed virtually no bone regeneration at the defect (Fig. 2A, B and Fig. S3). In contrast, femora that received OEhMSCs showed signs of new bone growth, but the newly formed tissue had random directionality (Fig. 2A, B and Fig. S3). Using the μCT scans, the volume of *de novo* bone was calculated at the defect. As expected, virtually no bone was detected in the

untreated and hMSC groups whereas a variable, but substantial amount of bone had formed in the OEhMSC treated group (Fig. 2C, D). Biomechanical testing of murine femora is technically challenging and uninformative in the absence of bone union. However, the polar moment of inertia (J), an estimation of the ability to resist torsion based on cross-sectional area and density, is a surrogate for biomechanical strength measurements in long bones (20, 21). Initially, measurements were taken from adjacent cross-sections at the proximal, distal (Fig. S4) and mid-point of the defects as defined by the edges of the pin collar (Fig. 2E). For the midline measurements, J was low in the untreated and hMSC treated groups but significantly higher in the OEhMSC treated group. Although variable, J measurements for the OEhMSC treated group was close to measurements attained for uninjured bones. In the case of proximal and distal measurements (Fig. S4), the value of J at the distal end of the injury reflected the results for the mid-line but in the case of the proximal measurements, all values were low. This confirms qualitative observations (Fig. 2A, Fig. S3) in that bone growth appeared to occur predominantly from the distal end. The mean values of J for the entire defect also indicated that more bone had formed in the OEhMSC treated group (Fig. 2F). These data confirmed that OEhMSCs were osteogenically superior to controls, but lacked directionality without a scaffold or support.

A cell retention scaffold from the ECM of OEhMSCs

We previously demonstrated that OEhMSC- derived ECM extended OEhMSC retention time in calvarial defects, resulting in enhanced healing (17). The drawback of this approach is that the OEhMSC-ECM is recoverable in yields too low to permit clinical use, but speculated that the volume of the ECM could be enhanced by coating it on existing scaffolds. We selected porcine gelatin foam (GF) due to its excellent MSC-adherence properties and common use in humans. To test whether it was possible to coat OEhMSC-ECM onto GF, we seeded 1×10^6 OEhMSCs onto 0.25 cm^3 pieces and monitored attachment and expansion. Initially, OEhMSCs readily adhered to the foam as visualized by immunohistochemistry (Fig. 3A). Over 22 days, ECM filled the cavities of the GF resulting in a stronger, denser construct (Fig. 3B, C). When the 22-day GF cultures were stained with live/dead stain, a confluent layer of viable OEhMSCs could be detected (Fig. 3E, F). The kinetics of cell growth on GF were biphasic in that there was a rapid accumulation of OEhMSCs up to day 5, a period where cell numbers diminish at day 14, and recovery of numbers at day 22 (Fig. 3D). After 22 days, the constructs were processed by detergent treatment, digestion with nucleases and trypsin, followed by washes in dH_2O, chloroform and acetone. The dried ECM/GF composite, hereafter referred to as *bioconditioned Gelfoam* (BGF), had the feel and appearance of decalcified bone tissue (Fig. 3G). Upon re-seeding with fresh OEhMSCs, the cells adhered and proliferated with kinetics similar to GF (Fig. 3H). Interestingly, when freshly seeded BGF/OEhMSC constructs were incubated in media containing DMSO, then frozen to −80°C, they could be recovered with 70% viability (Fig. 3H).

We then compared GF and BGF for their capacity to retain hMSCs and OEhMSCs in the femoral defect model. We shaped GF and BGF into cylinders that could be passed over the medullary pins (Fig. S1C) and administered hMSCs or OEhMSCs to the cylinders after implantation. After 3 weeks, mice were euthanized, limbs were scanned by μCT for bone

volume, surface area and J measurements (proximal, distal, midline and mean of the entire ROI). In the following experimental groups; GF alone, BGF alone, GF/hMSC, GF/OEhMSC, we observed modest levels of new bone growth (Fig. 4A–C). We also observed that OEhMSCs/GF constructs improved healing when compared to hMSC/GF constructs but rarely resulted in bridging of the defect. Histological analysis confirmed that the majority of tissue at the site of the defects took the form of fibrous, non-ossified matrix (Fig. 5A–C) with the exception of the GF/OEhMSC group where a small amount of immature osteoid accompanied by areas of mineralization could be detected (Fig. 5D).

OEhMSCs then were combined with BGF in an effort to extend the retention time of the OEhMSCs at the injury (17). In contrast with the previous conditions, the combination of BGF/OEhMSCs resulted in complete bridging in over 60% of subjects (as indicated by axial and 3D reconstructions of μCT scans) and a statistically significant improvement in μCT parameters (Figs. 4A–C, Fig. S5 and S6). While complete circumferential bone coverage was not evident in all cases, histology confirmed sufficient well-developed bone at the midline of the lesions to facilitate remodeling in each of the specimens (Fig. 5E).

BGF up-regulates BMP2 secretion

While OEhMSC-derived ECM appears to improve bone healing through collagen-mediated enhancement of cell retention (17), a direct role in improving function of osteoprogenitors has yet to be demonstrated. When seeded onto GF, OEhMSCs up-regulated a number of collagens enriched in developing bone (e.g. V (22), VI (23), XI (22), XII and XIV (24)) when compared to hMSCs (Fig. 6A). To address whether these developmental collagens might stimulate the secretion of osteogenic factors by OEhMSCs, we seeded them onto GF or BGF *in vitro*. After 5 days, we performed transcriptome micro-array analysis to identify genes that were up-regulated >2-fold. We then analyzed the list using the Database for Annotation, Visualization and Integrated Discovery (DAVID) application (25). DAVID identified up-regulation of 23 secreted osteogenic ligands, with bone morphogenic protein-2 (BMP2), cartilage oligomeric matrix protein (COMP), BMP8B and BMP6 up-regulated to the greatest degree (Table S2). DAVID also identified 8 angiogenic ligands (Table S3). Although the data suggested that BGF induced the secretion of a cocktail of osteogenic proteins, we directed our attention to BMP2, given its key role in osteogenesis and repair. ELISA assays confirmed secretion of BMP2 at 0.603 ± 0.153 fg·cell^{-1}·day^{-1} for OEhMSCs on GF, compared to 5.587 ± 0.326 fg·cell^{-1}·day^{-1} on BGF. We next interrogated the micro-array data for a potential mechanism for the up-regulation of BMP2 and found that integrin / focal adhesion signaling was strongly represented by the data (Figs. S7,8). Intriguingly collagen fibrils have the capacity to activate the integrin /focal adhesion kinase axis resulting in the expression of BMP2 (26). While many collagens have the capacity to activate do this, we noted a robust up-regulation of type VI and XII collagen protein in OEhMSCs when compared to hMSCs (Fig. 6A). This is significant because types VI and XII collagen localize to regenerating bone tissue (23, 24, 27) and deficits of collagen VI and XII in mice cause osteoblast abnormalities (28–30). It is therefore possible that type VI and XII collagen in BGF may induce expression of BMP2 by OEhMSCs, accounting for some of the beneficial effects of BGF in bone healing. To test this, we blocked type VI and/or type XII collagen by incubation of BGF with a polyclonal antibody. We then incubated OEhMSCs in

the presence of the antibody-treated BGF for a further 48 h and assayed BMP2 by qRT-PCR. We found that although OEhMSC attachment was not affected by antibody-treatment (Fig. 6B), immune-blockade of both type VI and type XII collagen reduced transcription of BMP2 (Fig. 6C). Together with the findings of our previous study (17), the data suggest that BGF acts in a dual manner by retaining osteoprogenitor cells at the site of injury for extended periods while inducing the expression of osteogenic and angiogenic ligands. This occurs in part, through collagen VI/XII-induced activation of BMP2 secretion by OEhMSCs and possibly endogenous osteoprogenitor cells.

Cryopreservation of OEhMSC/ECM composites retains viability and in vivo efficacy

To establish whether live OEhMSC/ECM composites could be cryopreserved, OEhMSCs were cultured on OEhMSC-derived ECM for 5 days. Composites of approximately 125 mm^3 were incubated in the presence of culture media containing 30% FBS and 5% DMSO then transferred to an isopropanol bath for cryopreservation at −80°C. After 48 h, composites were thawed to 37°C, washed in culture media and subjected to live/dead assay. Fluorescence microscopy confirmed a predominance of live cells, in agreement with similar assays performed on BGF/OEhMSC constructs (Figs. 7A, B and 3E, F).

Because cryopreservation and thawing damaged the fragile cylinders necessary for femoral repair assays, a murine calvarial lesion assay was performed to evaluate *in vivo* efficacy of the cryo-preserved constructs (16, 17). Constructs containing 500,000 cells were implanted into 4 mm diameter calvarial lesions in nude mice. After 3 weeks, calvaria were assayed by digital radiography. The extent of healing was quantified by densitometry using a healing index where 0 refers to no healing or complete radiolucency and 1 refers to radioopacity that is equivalent to the contralateral side. Healing was marginal in mice that received no treatment (*mock*) or ECM only, but in those that received either unfrozen or cryo-recovered ECM/OEhMSC composites, healing was between 60–80% of the contralateral side (Fig. 7C, D). The data obtained for both cryo-preserved and unfrozen composites were statistically equivalent suggesting that, at least for small constructs, the freezing process did not affect efficacy to a significant degree.

Discussion

Herein, we report a novel MSC-based composite for the repair of long-bone. MSCs are recovered from the bone marrow of healthy patients undergoing spinal fusion. After expansion they are cultured in conditions that induce an osteogenically enhanced phenotype *in vitro* (Fig. 1A–C). These conditions include basic osteogenic supplementation and an inhibitor of PPARγ. The effect of this induction protocol is to ablate inhibitory cross-talk from the adipogenic PPARγ axis so as to enhance cWnt signaling and thus initiate an early osteoprogenitor phenotype (16, 17). We have termed these cells *osteogenically enhanced hMSCs* (OEhMSCs).

To demonstrate efficacy of OEhMSCs *in vivo*, we devised a femoral segmental defect in nude mice. While several murine orthopedic models have been reported, they can be technically challenging to implement (31). Herein, we describe a simple femoral medullary pin with a central collar designed to prevent closing of the injury and also delineate the

original edges of the defect. While the pin was not fixed to the bone, precise sizing of the diameter results in sufficient interference to minimize torsional motion. The result is a *hypertrophic non-union defect* (32) which can be easily evaluated radiologically.

Initially, we found OEhMSCs in the presence of clotted plasma resulted in a large volume of new bone tissue at the defect that was not evident in hMSC controls (Fig. 2A, C). However, while the volume of newly formed bone was sufficient to bridge the gap, its formation occurred with unpredictable directionality, resulting in failure of union. While plasma can enhance osteogenesis by OEhMSCs (16) it was not suitable as a retention scaffold in segmental defects. Nevertheless it is attractive to speculate that percutaneous injection of OEhMSCs with plasma may be useful for the treatment of non-critical-sized bone injuries. Indeed, percutaneous administration of autologous whole bone marrow has been successfully used to repair non-union fractures (33).

To address the issue of retention, we provided a GF collar circumferentially positioned around the defect to enhance cell attachment and retention. GF was chosen because it is highly compatible with osteoblasts and MSCs, it is easy to handle, and is approved for clinical applications (34, 35). We then coated the GF with ECM derived from OEhMSCs prompted by our previous observations that the OEhMSC-derived ECM retained freshly administered OEhMSCs at the site of bone injuries for long durations, resulting in improved healing (17). GF was "*bioconditioned*" by OEhMSC-ECM by culture for 21 days, followed by decellularization by a series of enzyme, detergent and solvent treatments. The resultant material (bioconditioned Gelfoam, BGF) consisted of a dense material with the gross appearance and handling properties of decalcified bone. When OEhMSCs were re-seeded onto BGF *in vitro* (Fig 3H), biocompatibility surpassed commercial synthetic bone mimics (36). Importantly, the BGF-OEhMSC composites could be frozen and recovered while retaining *in vivo* efficacy suggesting that the constructs may be stored until required. When tested in the femoral defect model, BGF/OEhMSCs exhibited a markedly enhanced capacity to generate new bone and bridge defects (Fig. 4A–E). This suggested that BGF was acting in a similar manner as previously reported, causing extended retention of OEhMSCs, thus extending the duration of bone healing (17). Taken together, these data suggest that BGF/OEhMSC constructs may be an excellent allogeneic bone mimic.

While it appeared that the mechanism of BGF/OEhMSC was based on extended retention of viable OEhMSCs at the site of injury, we speculated that BGF may also enhance the functionality of OEhMSCs. Indeed, stem cells have been reported to differentiate into the appropriate cell-type when seeded onto to decellularized matrices from various tissues (37). Specifically, we tested whether OEhMSCs may be induced to secrete beneficial proteins at the site of injury. Given the absence of OEhMSCs in healed calvarial lesions as noted in our previous studies (16, 17), it was reasonable to assume the predominant mode of action was a bystander or trophic effect rather than direct contribution to tissue regeneration. In support of this hypothesis, we found that OEhMSCs expressed numerous osteogenic and angiogenic protein ligands when attached to BGF *in vitro* compared to GF alone (Tables S2 and S3). Most notably, BMP2 was highly upregulated at the level of transcription and secreted protein. Bioinformatic analysis confirmed a predominance of integrin-mediated signal transduction in OEhMSCs attached to BGF (Figs. S7 and S8), suggesting that this might be

the mechanism for upregulated BMP2 production. Indeed, integrin engagement and mitogen activated protein kinase signaling have been reported to induce BMP2 expression and osteogenic differentiation (26).

While BGF is a complicated cocktail of ECM molecules that is likely to act in numerous interconnected ways, OEhMSCs upregulate minor collagen components that are enriched in highly anabolic bone tissue (17, 23, 24). In particular, we found type VI and XII collagens to be highly upregulated (Fig. 6A, B). This is of interest because both collagens have been shown to be essential for osteoblast function (28–30, 38). Accordingly, we found that immunoblockade of either collagen in BGF reduced transcription of BMP2 by OEhMSCs without affecting their attachment. Currently, the mechanism responsible for collagen VI/XII mediated regulation of BMP2 is not understood, but both collagens possess von Willebrand factor A (VWFA) modules (39). Since VWFA is known to sequester OPG (40), it is attractive to speculate that VWFA:OPG complexes may be responsible for enhancement of osteogenic activity and associated BMP2 production.

Finally, we observed that OEhMSCs could be cryopreserved while attached to BGF with no significant detriment to cell viability (Fig. 3H). Critically, when OEhMSCs were attached to OEhMSC-derived ECM (in this instance, the ECM was pure, rather than coated onto GF), recovered after cryopreservation, and implanted into defects of murine calvaria, bone healing was robust (approximately 80% closure of the defect) and equivalent to freshly prepared OEhMSC/ECM constructs. These data raise the exciting possibility of cryopreserved tissue repair constructs that could be utilized at the point of care without requiring significant periods of subculture.

Supplementary Material

Refer to Web version on PubMed Central for supplementary material.

Acknowledgments

We thank the Scott & White Hospital Blood Center team (director: Walter Linz, MD) for the supply of PBLs.

Funding: This work was funded in part by The Institute for Regenerative Medicine Program Funds, Scott & White RGP grants #90172 and #100216, project grants from the Center for Advancement of Science in Space (CASIS) and the North American Spine Society (NASS), and NIH 2P40RR017447-07.

References

1. Tzioupis C, Giannoudis PV. Prevalence of long-bone non-unions. Injury. 2007; 38 (Suppl 2):S3–9. [PubMed: 17920415]
2. Boden SD. Biology of lumbar spine fusion and use of bone graft substitutes: present, future, and next generation. Tissue Eng. 2000; 6(4):383–99. [PubMed: 10992434]
3. Green E, Lubahn JD, Evans J. Risk factors, treatment, and outcomes associated with nonunion of the midshaft humerus fracture. J Surg Orthop Adv. 2005; 14(2):64–72. [PubMed: 16115430]
4. Kanakaris NK, Giannoudis PV. The health economics of the treatment of long-bone non-unions. Injury. 2007; 38 (Suppl 2):S77–84. [PubMed: 17920421]
5. Ibrahim T, Stafford H, Esler CN, Power RA. Cadaveric allograft microbiology. Int Orthop. 2004; 28(5):315–8. [PubMed: 15480661]

6. Kao ST, Scott DD. A review of bone substitutes. Oral Maxillofac Surg Clin North Am. 2007; 19(4): 513–21. vi. [PubMed: 18088902]
7. Shegarfi H, Reikeras O. Review article: bone transplantation and immune response. J Orthop Surg (Hong Kong). 2009; 17(2):206–11. [PubMed: 19721154]
8. Hiremath GK, Steinmetz MP, Krishnaney AA. Is it safe to use recombinant human bone morphogenetic protein in posterior cervical fusion? Spine (Phila Pa 1976). 2009; 34(9):885–9. [PubMed: 19531997]
9. Wong DA, Kumar A, Jatana S, Ghiselli G, Wong K. Neurologic impairment from ectopic bone in the lumbar canal: a potential complication of off-label PLIF/TLIF use of bone morphogenetic protein-2 (BMP-2). Spine J. 2008; 8(6):1011–8. [PubMed: 18037352]
10. Robin BN, Chaput CD, Zeitouni S, Rahm MD, Zerris VA, Sampson HW. Cytokine-mediated inflammatory reaction following posterior cervical decompression and fusion associated with recombinant human bone morphogenetic protein-2: a case study. Spine (Phila Pa 1976). 2010; 35(23):E1350–4. [PubMed: 20938385]
11. Cuomo AV, Virk M, Petrigliano F, Morgan EF, Lieberman JR. Mesenchymal stem cell concentration and bone repair: potential pitfalls from bench to bedside. J Bone Joint Surg Am. 2009; 91(5):1073–83. [PubMed: 19411455]
12. Rihn JA, Kirkpatrick K, Albert TJ. Graft options in posterolateral and posterior interbody lumbar fusion. Spine (Phila Pa 1976). 2010; 35(17):1629–39. [PubMed: 20628336]
13. Krause U, Gregory CA. Potential of Modulating Wnt Signaling Pathway Toward the Development of Bone Anabolic Agent. Curr Mol Pharmacol. 2011
14. Farmer SR. Regulation of PPARgamma activity during adipogenesis. Int J Obes (Lond). 2005; 29 (Suppl 1):S13–6. [PubMed: 15711576]
15. Seimandi M, Lemaire G, Pillon A, Perrin A, Carlavan I, Voegel JJ, et al. Differential responses of PPARalpha, PPARdelta, and PPARgamma reporter cell lines to selective PPAR synthetic ligands. Anal Biochem. 2005; 344(1):8–15. [PubMed: 16038868]
16. Krause U, Harris S, Green A, Ylostalo J, Zeitouni S, Lee N, et al. Pharmaceutical modulation of canonical Wnt signaling in multipotent stromal cells for improved osteoinductive therapy. Proc Natl Acad Sci U S A. 2010; 107(9):4147–52. [PubMed: 20150512]
17. Zeitouni S, Krause U, Clough BH, Halderman H, Falster A, Blalock DT, et al. Human mesenchymal stem cell-derived matrices for enhanced osteoregeneration. Sci Transl Med. 2012; 4(132):132ra55.
18. Gregory, CA.; Prockop, DJ. Fundementals of Culture and Characterization of Mesenchymal Stem/ Progenitor Cells from Bone Marrow Stroma. In: Freshney, RIS.; GN; Auerbach, JM., editors. Culture of Human Stem Cells. Hoboken NJ: Wiley-Liss; 2007. p. 208
19. Dominici M, Le Blanc K, Mueller I, Slaper-Cortenbach I, Marini F, Krause D, et al. Minimal criteria for defining multipotent mesenchymal stromal cells. The International Society for Cellular Therapy position statement. Cytotherapy. 2006; 8(4):315–7. [PubMed: 16923606]
20. O'Neill KR, Stutz CM, Mignemi NA, Burns MC, Murry MR, Nyman JS, et al. Micro-computed tomography assessment of the progression of fracture healing in mice. Bone. 2012; 50(6):1357–67. [PubMed: 22453081]
21. Bagi CM, Hanson N, Andresen C, Pero R, Lariviere R, Turner CH, et al. The use of micro-CT to evaluate cortical bone geometry and strength in nude rats: correlation with mechanical testing, pQCT and DXA. Bone. 2006; 38(1):136–44. [PubMed: 16301011]
22. Yamazaki M, Majeska RJ, Yoshioka H, Moriya H, Einhorn TA. Spatial and temporal expression of fibril-forming minor collagen genes (types V and XI) during fracture healing. J Orthop Res. 1997; 15(5):757–64. [PubMed: 9420607]
23. Marvulli D, Volpin D, Bressan GM. Spatial and temporal changes of type VI collagen expression during mouse development. Dev Dyn. 1996; 206(4):447–54. [PubMed: 8853993]
24. Walchli C, Koch M, Chiquet M, Odermatt BF, Trueb B. Tissue-specific expression of the fibril-associated collagens XII and XIV. J Cell Sci. 1994; 107 (Pt 2):669–81. [PubMed: 8207089]
25. Huang da W, Sherman BT, Lempicki RA. Systematic and integrative analysis of large gene lists using DAVID bioinformatics resources. Nat Protoc. 2009; 4(1):44–57. [PubMed: 19131956]

26. Lu Z, Zreiqat H. The osteoconductivity of biomaterials is regulated by bone morphogenetic protein 2 autocrine loop involving α2β1 integrin and mitogen-activated protein kinase/extracellular related kinase signaling pathways. Tissue Eng Part A. 2010; 16(10):3075–84. [PubMed: 20575676]
27. Hiltunen A, Metsäranta M, Perälä M, Säämänen AM, Aro HT, Vuorio E. Expression of type VI, IX and XI collagen genes and alternative splicing of type II collagen transcripts in fracture callus tissue in mice. FEBS Lett. 1995; 364(2):171–4. [PubMed: 7750564]
28. Christensen SE, Coles JM, Zelenski NA, Furman BD, Leddy HA, Zauscher S, et al. Altered trabecular bone structure and delayed cartilage degeneration in the knees of collagen VI null mice. PLoS One. 2012; 7(3):e33397. [PubMed: 22448243]
29. Izu Y, Ezura Y, Mizoguchi F, Kawamata A, Nakamoto T, Nakashima K, et al. Type VI collagen deficiency induces osteopenia with distortion of osteoblastic cell morphology. Tissue Cell. 2012; 44(1):1–6. [PubMed: 22071216]
30. Izu Y, Sun M, Zwolanek D, Veit G, Williams V, Cha B, et al. Type XII collagen regulates osteoblast polarity and communication during bone formation. J Cell Biol. 2011; 193(6):1115–30. [PubMed: 21670218]
31. Holstein JH, Garcia P, Histing T, Kristen A, Scheuer C, Menger MD, et al. Advances in the establishment of defined mouse models for the study of fracture healing and bone regeneration. J Orthop Trauma. 2009; 23(5 Suppl):S31–8. [PubMed: 19390374]
32. Garcia P, Histing T, Holstein JH, Klein M, Laschke MW, Matthys R, et al. Rodent animal models of delayed bone healing and non-union formation: a comprehensive review. Eur Cell Mater. 2013; 26:1–12. discussion -4. [PubMed: 23857280]
33. Hernigou P, Poignard A, Beaujean F, Rouard H. Percutaneous autologous bone-marrow grafting for nonunions. Influence of the number and concentration of progenitor cells. J Bone Joint Surg Am. 2005; 87(7):1430–7. [PubMed: 15995108]
34. Rohanizadeh R, Swain MV, Mason RS. Gelatin sponges (Gelfoam) as a scaffold for osteoblasts. J Mater Sci Mater Med. 2008; 19(3):1173–82. [PubMed: 17701305]
35. Bilousova G, Jun dH, King KB, De Langhe S, Chick WS, Torchia EC, et al. Osteoblasts derived from induced pluripotent stem cells form calcified structures in scaffolds both in vitro and in vivo. Stem Cells. 2011; 29(2):206–16. [PubMed: 21732479]
36. Murphy MB, Suzuki RK, Sand TT, Chaput CD, Gregory CA. Short Term Culture of Human Mesenchymal Stem Cells with Commercial Osteoconductive Carriers Provides Unique Insights into Biocompatibility. Journal of Clinical Medicine. 2013; 2(3):49–66.
37. Yin Z, Chen X, Zhu T, Hu JJ, Song HX, Shen WL, et al. The effect of decellularized matrices on human tendon stem/progenitor cell differentiation and tendon repair. Acta Biomater. 2013; 9(12): 9317–29. [PubMed: 23896565]
38. Atkinson JC, Rühl M, Becker J, Ackermann R, Schuppan D. Collagen VI regulates normal and transformed mesenchymal cell proliferation in vitro. Exp Cell Res. 1996; 228(2):283–91. [PubMed: 8912722]
39. Bork P. The modular architecture of vertebrate collagens. FEBS Lett. 1992; 307(1):49–54. [PubMed: 1639194]
40. Shahbazi S, Lenting PJ, Fribourg C, Terraube V, Denis CV, Christophe OD. Characterization of the interaction between von Willebrand factor and osteoprotegerin. J Thromb Haemost. 2007; 5(9):1956–62. [PubMed: 17723135]

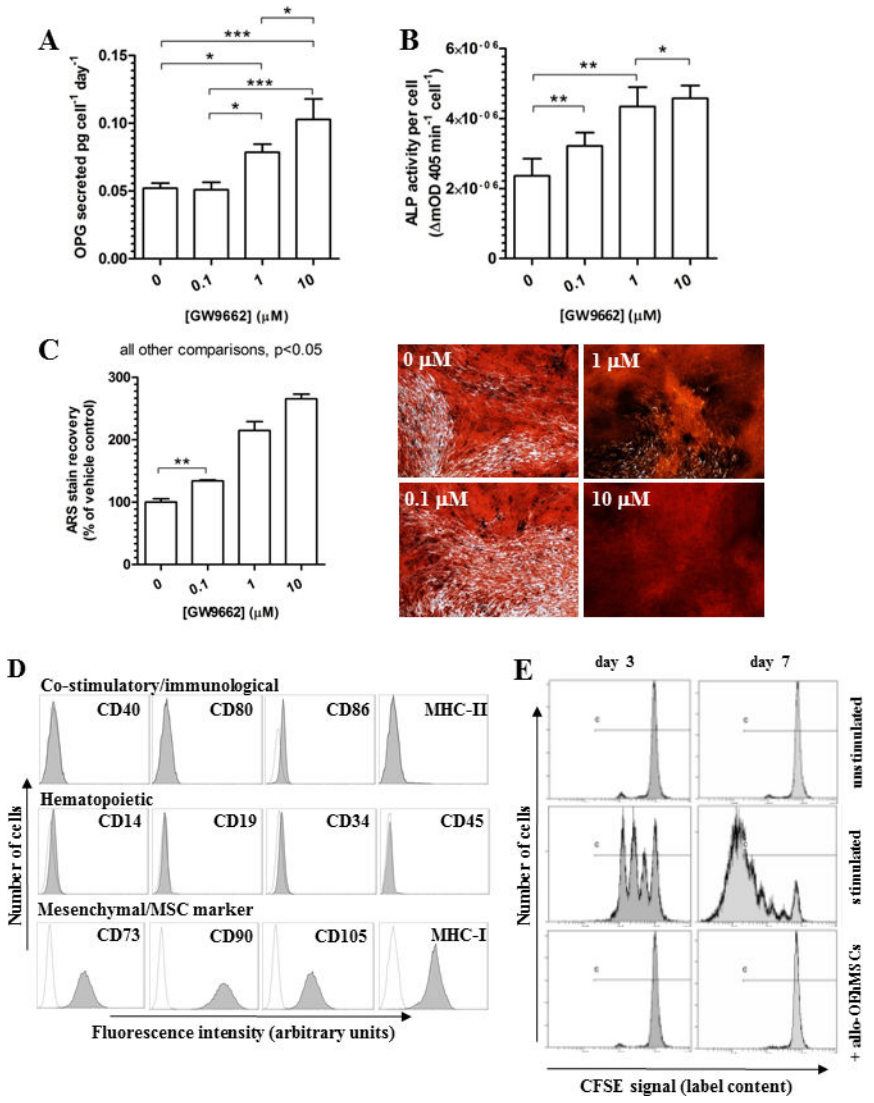

Fig. 1. Characterization of OEhMSCs

Human MSCs were incubated in osteogenic base media in the presence of various concentrations of GW9662 for 4 (**panel A**), 8 (**panel B**) and 21 days (**panel C**). **Panel A:** Measurement of OPG secretion by ELISA in response to GW9662 exposure. **Panel B:** Measurement of ALP activity by colorimetric assay in response to GW9662 exposure. **Panel C:** Measurement of deposition of a mineralized matrix by alizarin red staining by microscopy (**right panel**) and spectrophotometric quantification following extraction (**left panel**) in response to simultaneous dexamethasone and GW9662 exposure. **Panel D:** immunophenotype of OEhMSCs after 21 days of exposure to 10 μM GW9662 in the presence of osteogenic base media. Data represent means (n=3) with error bars representing standard deviations. **Panel E:** Immunologically mismatched PBLs were labeled with CFSE and incubated with OEhMSC (1:10 OEhMSC:PBL), CD3/CD28 beads (stimulated) or media alone (unstimulated). Cells were then analyzed by flow cytometry. OEhMSCs do not stimulate lymphocyte expansion as demonstrated by lack of dye dilution. Statistical testing

was performed by ANOVA and Tukey post-test. *P*-values key: $P<0.05$ = *, $P<0.01$=**, $P<0.005$=***.

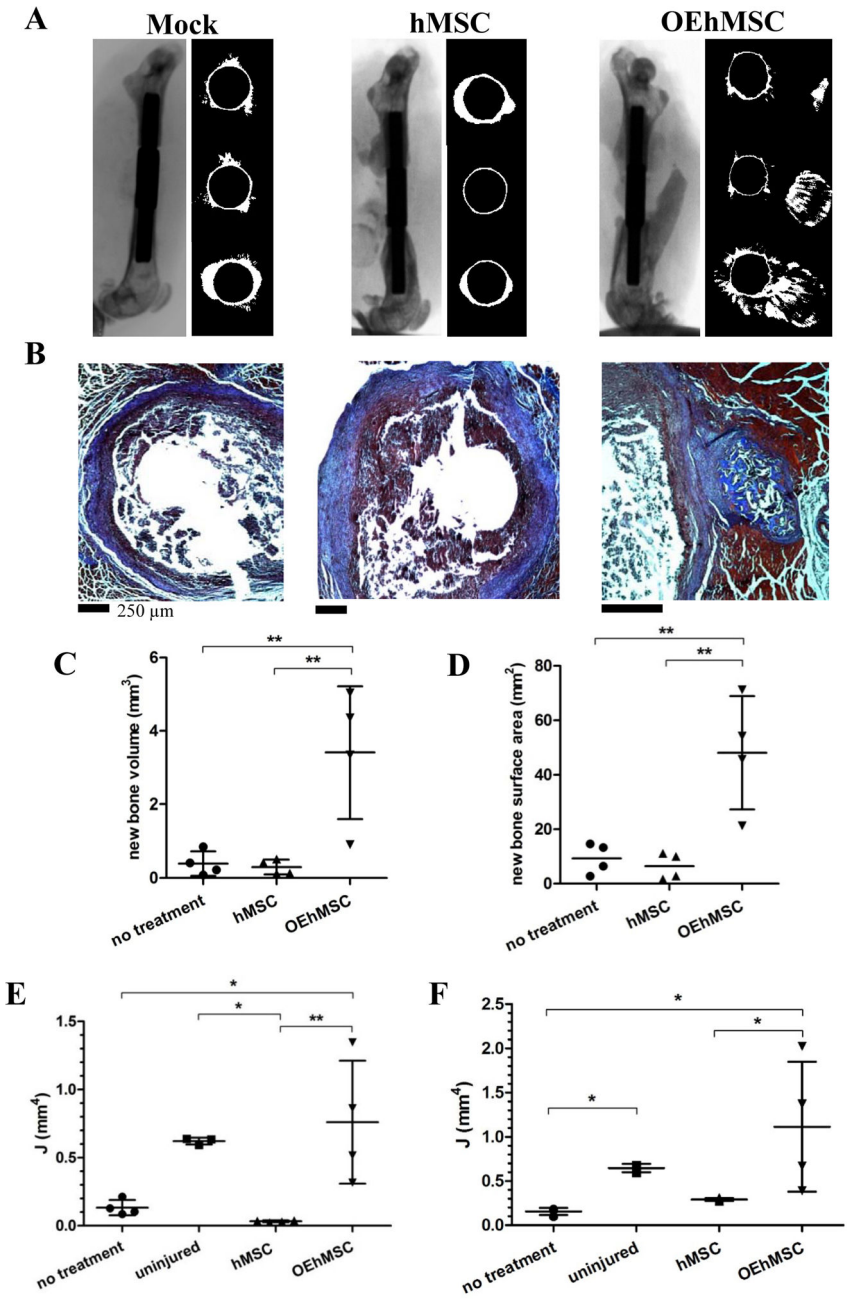

Fig. 2. A comparison of directly administered hMSCs and OEhMSCs for healing a critical-sized segmental defect of the femur and allowed to heal for 2 weeks

MSCs were directly administered to pin-stabilized defects in the presence of clotting plasma only. **Panel A:** μCT scans (left) and axial reconstructions of the proximal edge of the defect, (top right), mid-defect (center right) and distal edge of the defect (bottom right). **Panel B:** paraffin embedded axial sections stained with Masson's trichrome corresponding to the mid-defect. **Panel C and D:** measurements of new bone volume (**panel C**) and new bone surface area (**panel D**) between the original edges of the defect calculated by μCT-rendered reconstructions. **Panel E:** measurements of the polar moment of inertia (J) at the mid-defect (values are generated by taking the mean of 3 adjacent axial images). **Panel F**: the mean

value of J for the entire ROI. Statistical testing was performed by ANOVA and Tukey post-test. *P*-values key: $P<0.05$ = *, $P<0.01$=**, $P<0.005$=***.

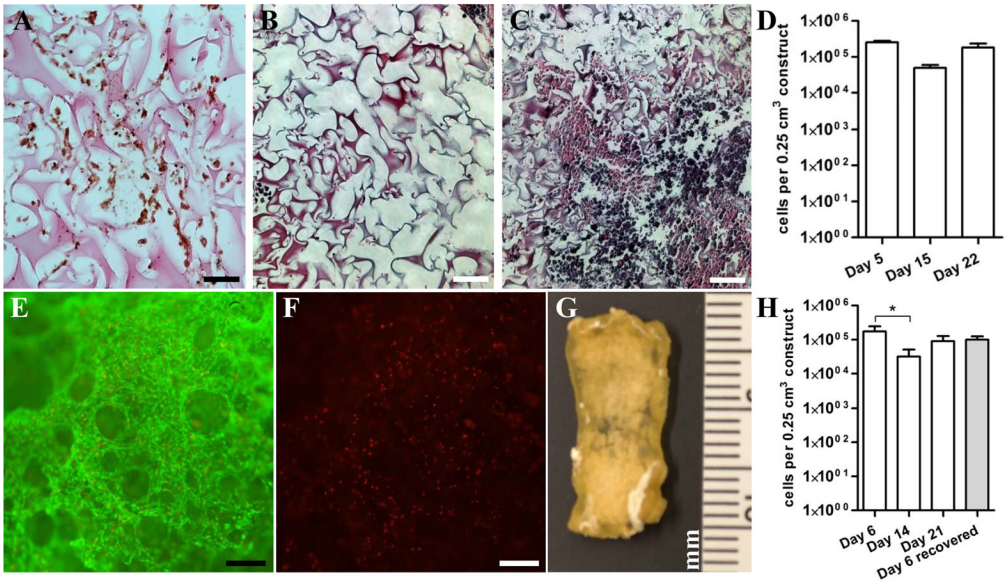

Fig. 3. Characterization of BGF production and OEhMSC re-seeding

Panel A: Paraffin embedded section of GF 5 days after seeding with OEhMSCs. GF is counterstained with eosin and OEhMCSs are stained with an antibody against human β-2 microglobulin. Staining is visualized by the peroxidase/diaminobenzidine technique. **Panel B and C:** Paraffin embedded section of GF 5 days (**panel B**) and 21 days (**panel C**) after seeding with OEhMSCs stained with hematoxylin and eosin. **Panel D:** The population of OEhMSCs on the GF measured by qRT-PCR for GAPDH, and compared with known standards. **Panel E and F:** Live/dead staining of OEhMSCs present on the GF after 21 days of culture demonstrating an abundance of live (green stain, **panel E**) cells and sparsely distributed dead (red stain, **panel F**) cells. **Panel G:** gross appearance of decellularized, processed BGF. **Panel H:** The population of OEhMSCs re-seeded onto the BGF measured by qRT-PCR for GAPDH. The grey bar represents OEhMSCs seeded onto BGF for 5 days, frozen in cryoprotectant at −80°C, and then recovered by incubation in culture media for 24h. Bars: A-C = 50 μm; E, F = 125 μm

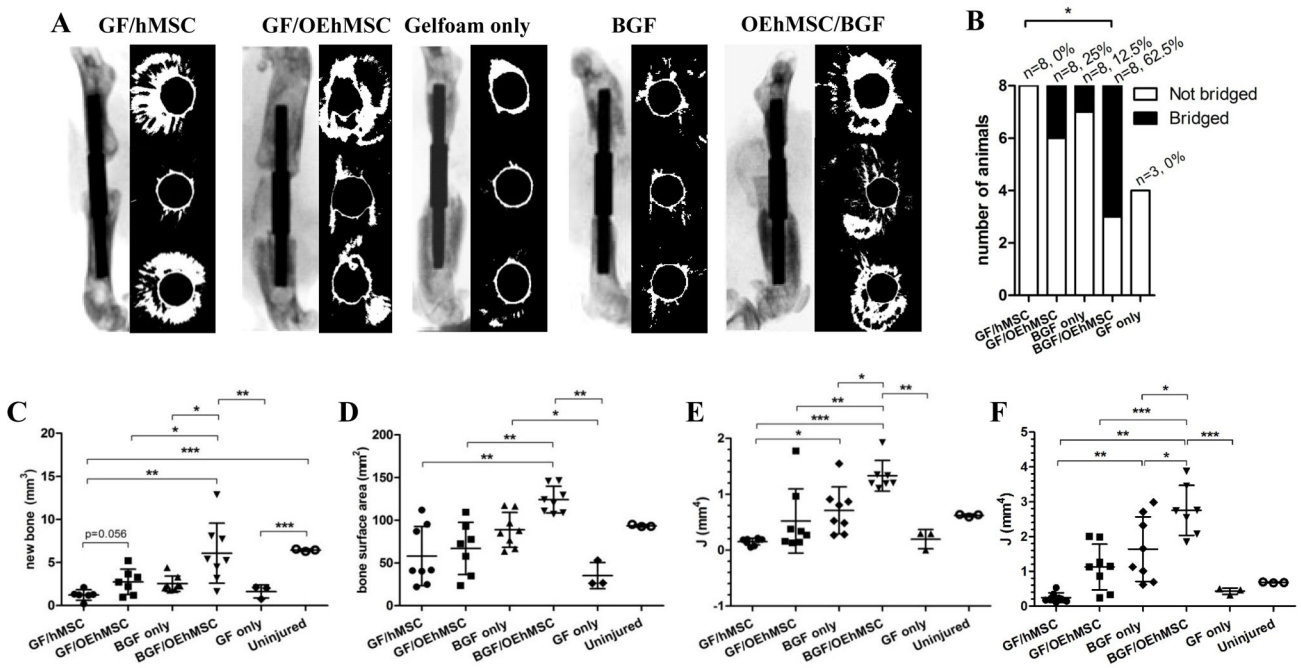

Fig. 4. A comparison of various combinations of hMSCs, OEhMSCs with GF or BGF for healing a critical-sized segmental defect of the femur

MSCs were directly administered to constructs (GF or BGF) in the presence of clotting plasma and allowed to heal for 3 weeks. **Panel A:** λCT scans and axial reconstructions presented as in Fig. 2A. **Panel B:** defect bridging defined by the presence of contiguous uninterrupted bone between the original edges of the defect. Statistics, Fisher Exact test (P<0.05=*). **Panels C–E:** Measurements of new bone volume (**panel C**), new bone surface area (**panel D**) and J measurements at the midline of the defect (**panel E**) and mean J for the entire ROI (**panel F**). Statistical testing was performed by ANOVA and Tukey post-test. *P*-values key: P<0.05 = *, P<0.01=**, P<0.005=***.

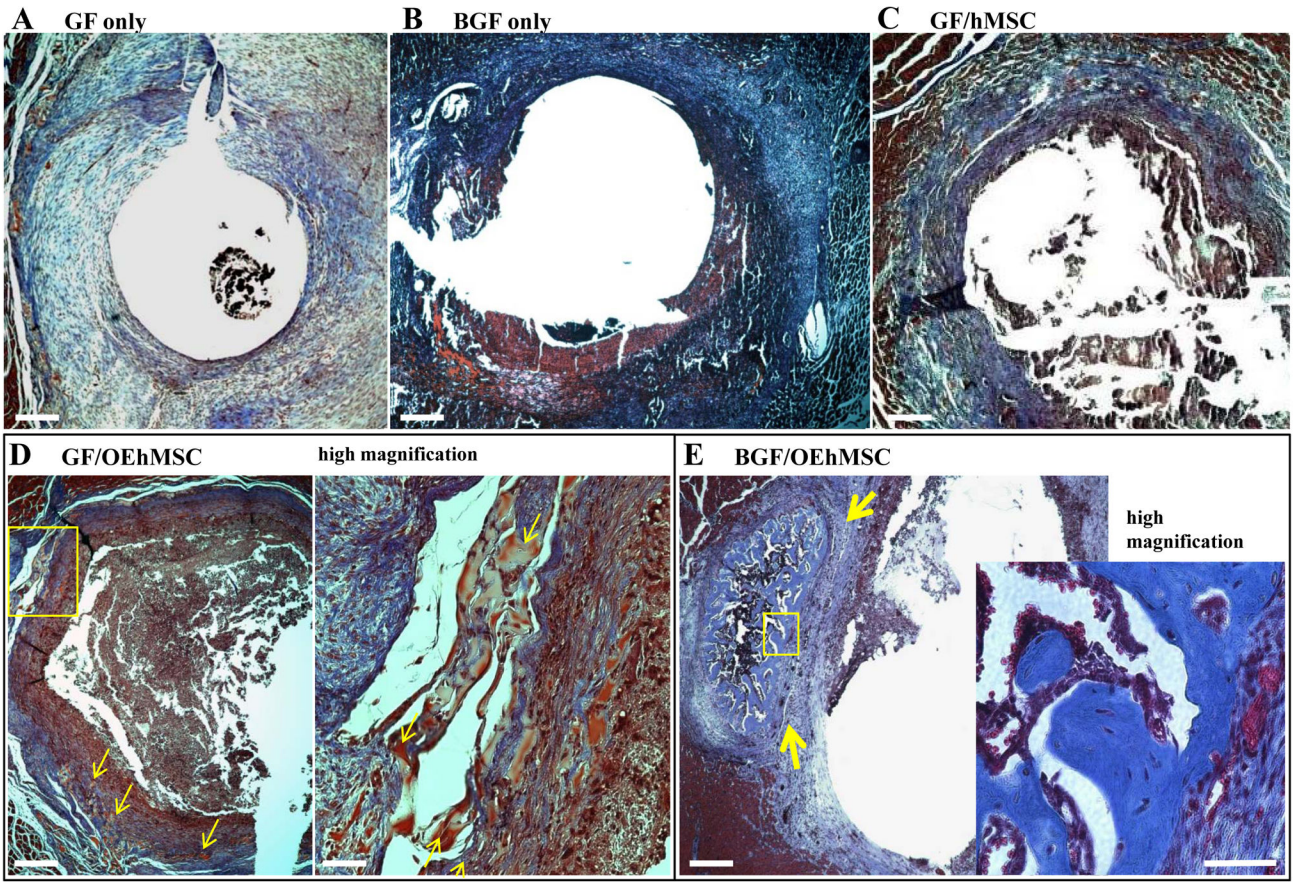

Fig. 5. Histological evaluation of healing femur samples scanned in Fig. 4

Decalcified and paraffin embedded femurs were sectioned in the axial orientation and stained with Masson's Trichrome to visualize new osteoid and mature bone. All sections represent the mid-point of the defect. **Panel A:** Low power micrograph of GF specimen demonstrating minimal bone formation, and deposition of blue fibrous tissue. **Panel B and C:** Low power micrographs of BGF-treated (panel B) and GF/hMSC-treated (panel C) specimens demonstrating presence of fibrous tissue but no bone is evident. **Panel D:** Low power micrograph (*left*) of GF/OEhMSC specimen demonstrating sporadic formation of red-stained primitive bone tissue (*arrowed*) shown in greater detail at high magnification (*right*). **Panel E:** Low power micrograph of bridged defect treated with a BGF/OEhMSC construct demonstrating the presence of mature trabecular bone at the midline of the defect (blue stain, *arrowed*). Inset (*below right*) is a high power micrograph of newly formed bone demonstrating normal histological appearance and cellularity. Low power images, bar = 250 μm, high power images, bar=25 μm.

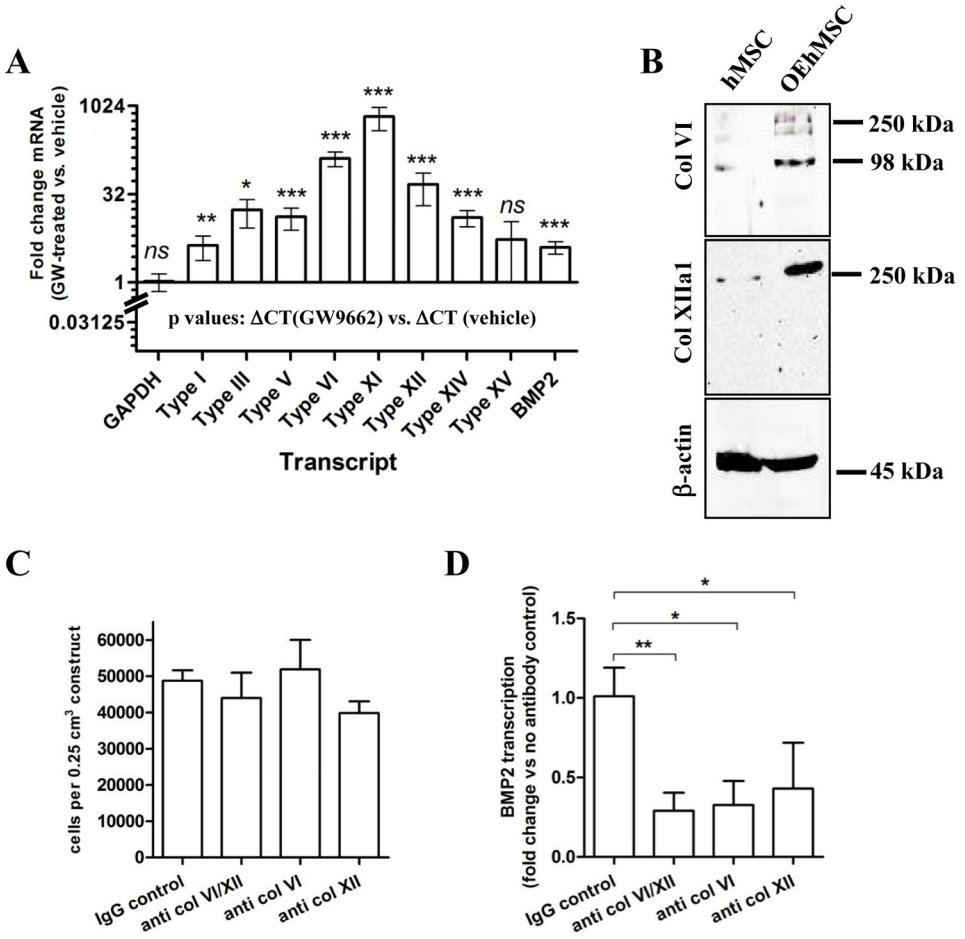

Fig. 6. Partial characterization of the mechanism of BGF

Panel A: Quantitative RT-PCR demonstrating upregulated transcription of collagen molecules enriched in anabolic bone tissue. Data are presented as fold-change in transcription between OEhMSCs and hMSCs. BMP2 secretion is also upregulated in OEhMSCs. **Panel B:** Immunoblot demonstrating up-regulation of type VI and type XII collagen expression in OEhMSCs. **Panel C:** Attachment of OEhMSCs to BGF unaffected by immune-blockade of type VI or type XII collagen. **Panel D:** Transcription of BMP2 by OEhMSCs is significantly reduced by immune-blockade of both type VI and type XII collagen.

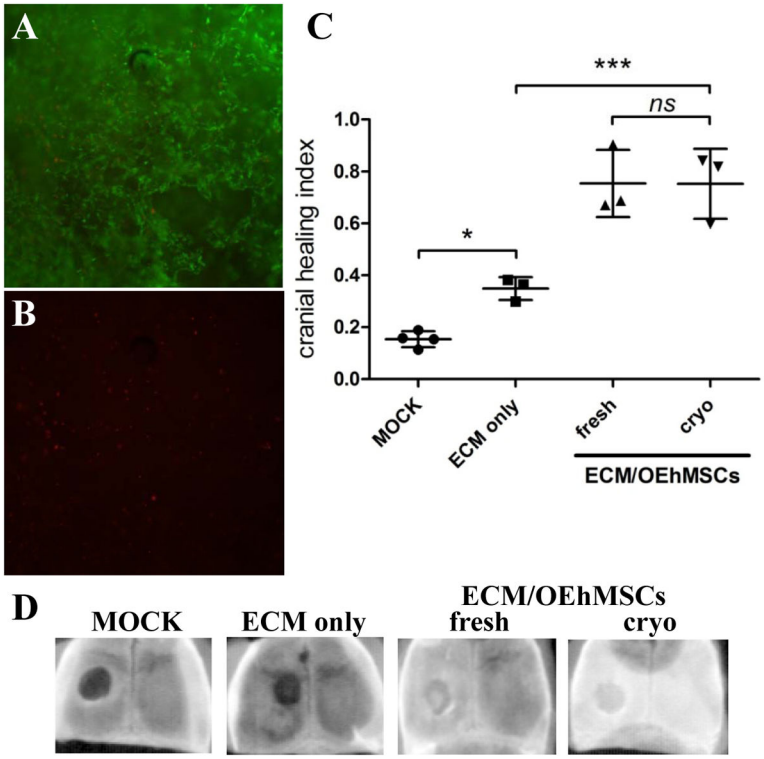

Fig. 7. Cryopreservation and recovery of ECM/OEhMSC constructs

Panel A and B: Live/dead assay on ECM/OEhMSC constructs recovered from cryopreservation at −80°C. Composite green (live cells) and red (dead cells) demonstrate predominance of live cells (panel A) and sparse distribution of dead cells (panel B). **Panel C:** ECM/OEhMSC constructs were frozen in cryo-protectant for 7 days (cryo) and thawed to 37°C or remained at 37°C with no freezing (fresh). The constructs were then administered to a 4 mm experimental defect of the cranium in nude mice. In 3 weeks, mice were euthanized and scanned by digital radiography. Healing index refers to the degree of radio-opacity as compared to the unlesioned contralateral side (1 = completely healed, 0 = no healing). Statistics: ANOVA with Tukey post-test (n=4), $P<0.05$ =*, $P<0.005$ =***. **Panel D:** Representative radiographs of calvaria used to generate data in panel C.